Title	Homo- and heteronuclear two-dimensional covariance solid-state NMR spectroscopy with a dual-receiver system.
Author(s)	Takeda, Kazuyuki; Kusakabe, Yasushi; Noda, Yasuto; Fukuchi, Masashi; Takegoshi, K
Citation	Physical chemistry chemical physics : PCCP (2012), 14(27): 9715-9721
Issue Date	2012-07-21
URL	http://hdl.handle.net/2433/189439
Right	This journal is © the Owner Societies 2012
Type	Journal Article
Textversion	author

Homo- and heteronuclear two-dimensional covariance solid-state NMR spectroscopy with a dual-receiver system

Kazuyuki Takeda,* Yasushi Kusakabe, Yasuto Noda, Masashi Fukuchi, and K. Takegoshi

Division of Chemistry, Graduate School of Science,

Kyoto University, 606-8502 Kyoto, Japan

(Dated: May 10, 2012)

Abstract

Two-dimensional (2D) covariance NMR spectroscopy, which has originally been established to extract homonuclear correlations (HOMCOR), is extended to include heteronuclear correlations (HETCOR). In a $^{13}C/^{15}N$ 2D chemical shift correlation experiment, ^{13}C and ^{15}N signals of a polycrystalline sample of ^{13}C, ^{15}N-labeled amino acid are acquired simultaneously using a dual-receiver NMR system. The data sets are rearranged for the covariance data processing, and the ^{13}C-^{15}N heteronuclear correlations are obtained together with the ^{13}C-^{13}C and ^{15}N-^{15}N homonuclear correlations. The present approach retains the favorable feature of the original covariance HOMCOR that the spectral resolution along the indirect dimension is given by that of the detection dimension. As a result, much fewer amounts of data are required to obtain a well-resolved 2D spectrum compared to the case of the conventional 2D Fourier-Transformation (FT) scheme. Hence, one can significantly save the experimental time, or enhance the sensitivity by increasing the number of signal averaging within a given measurement time.

INTRODUCTION

Two-dimensional (2D) Fourier-transform (FT) NMR spectroscopy has been widely used to characterize structure and dynamics of molecules of chemical/biological interest in solution and solids. One drawback in NMR spectroscopy in general is the low sensitivity. When a free induction decay (FID) has to be averaged over many times to attain tolerable signal-to-noise ratio, 2D FT NMR analysis becomes time consuming, as it requires a relatively long array of one-dimensional (1D) FIDs. In order to reduce the experimental time, alternative approaches have been proposed. They include Hadamard spectroscopy[1, 2] and covariance spectroscopy[3, 4]. Application of the former is restricted to samples with well-resolved Lorenzian or Gaussian lines, whereas the latter does not require any assumption on the resonance-line shape, and thus has wider potential applications in both liquid- and solid-state NMR.

Covariance is a concept in statistics, serving for a measure of how much a pair of variables are correlated with each other. Originally, the idea of covariance was introduced in IR and Raman spectroscopy[5]. Its application to NMR spectroscopy has been put forth by Brüschweiler and Zhang[3, 4], who demonstrated homonuclear correlation (HOMCOR) experiments in solution. Then, its feasibility for solid-state NMR was demonstrated by Hu et al[6]. Recently, covariance HOMCOR has also been applied to microcrystalline proteins[7] and study of binding of curcumin to amyloid β fibrils[8]. The experimental procedure is same for both 2D FT and covariance HOMCOR, in which an array of FIDs is acquired. In contrast to the former that performs 2D FT, data processing of the latter involves FT only in the direct dimension. Then, covariance is calculated for every pair of data points at given frequencies to evaluate if the relevant pair of magnetizations vary in a correlated way during the indirect dimension.

Meanwhile, a modified scheme was introduced, in which a 2D HOMCOR spectrum is calculated not by the covariance processing of an array of 1D spectra, but by that of a 2D FT spectrum. Such "indirect" covariance NMR spectroscopy was demonstrated both in solution[9] and in solids[10]. Snyder et al. applied covariance to a 4D NOESY spectrum[11]. They also established a general approach for indirect covariance that allows one to construct a covariance matrix from multiple NMR spectra[12]. In addition, Lafon et al. applied covariance to non-uniform sampling of natural abundance deuterium NMR data sets, halving

the measurement time compared with the original covariance scheme[13].

In the context of "direct" covariance NMR spectroscopy, only HOMCOR has been performed so far, although reducing the measurement time is also of interest for heteronuclear correlation (HETCOR) experiments. This is presumably due to the symmetric nature of the proposed covariance processing, which is suitable for HOMCOR but not for HETCOR. In this work, we show that covariance can be used to obtain the correlation between heteronuclear spins I and S, together with the I-I and S-S homonuclear correlations. We demonstrate experiments and covariance data processing in ^{1}H-^{1}H dipolar-coupling mediated ^{13}C/^{15}N chemical shift correlation experiments[14, 15], to obtain the ^{13}C-^{15}N heteronuclear correlation as well as the ^{13}C-^{13}C and ^{15}N-^{15}N homonuclear correlations.

In the ^{1}H-^{1}H dipolar-coupling mediated ^{13}C/^{15}N chemical shift correlation experiments, the ^{13}C and ^{15}N spins exchange their magnetizations through ^{1}H spin diffusion. The resultant 2D correlation spectra, often called CHHC, NHHN, and CHHN/NHHC spectra, tell the presence of such ^{1}H spins that are spatially close to the relevant ^{13}C/^{15}N spins. Until recently, acquisition of the ^{13}C and ^{15}N signals was done in separate implementations of the experiments. To save the experimental time, Herbst et al. employed a spectrometer with multiple receivers to acquire ^{13}C and ^{15}N FIDs simultaneously[16]. As shown below, one can also fully exploit the benefits of covariance CHHC, NHHN, and NHHC correlations by simultaneous measurements of the ^{13}C and ^{15}N signals using the dual-receiver system.

PRINCIPLE

Here, we show how the idea of covariance NMR can be extended to include heteronuclear correlations. Let us suppose for a moment that the signals from two nuclear spin species were detectable through one rf channel with a frequency bandwidth that would be large enough to cover the resonances of both spin species altogether. Then, the peaks from both species would appear in a single 1D spectrum, and the situation would be qualitatively the same as that in the established covariance HOMCOR analysis, and its straightforward application would give the correlations among the different spin species as well as among the same species. In practice, however, it is difficult to accommodate resonance frequencies of heteronuclear spins in a bandwidth of one rf channel. What we aim here is to reconfigure two heteronuclear signals acquired through the separate channels to form a single fictitious

spectrum containing both, so that the covariance analysis can be performed just in the same way as in the case of the covariance HOMCOR spectroscopy.

Fig. 1 shows a pulse sequence for the ^{1}H-^{1}H dipolar-coupling mediated ^{13}C/^{15}N chemical shift correlation experiment. First, the magnetizations of I (^{13}C) and S (^{15}N) spin species are enhanced by cross polarization (CP), and then stored along the z axis by applying $\pi/2$ pulses. After eliminating the ^{1}H magnetization by a z-filter, another $\pi/2$ pulse is applied to each of the I and S rf channels, letting the I and S spins evolve during the t_1 period under ^{1}H decoupling. The second CP process serves for passing the I and S magnetizations back to the ^{1}H spins, which, during the mixing time, undergo spin diffusion, exchanging the magnetizations with the nearby ^{1}H spins. Finally, another CP is performed, and the resultant I and S magnetizations are observed simultaneously using the dual-receiver system under ^{1}H decoupling.

In order to avoid spectral overlap of ^{13}C and ^{15}N resonances in the indirect dimension, time proportional phase increment (TPPI) is applied to phases $\varphi_{1\mathrm{C}}$ and $\varphi_{1\mathrm{N}}$, so that the frequencies of evolution are shifted during t_1. In addition, in order to retrieve the correct sign of the frequency of spin precession during the evolution time, a quadrature set of data are acquired for each value of t_1. This is done by the conventional States method[17], that is, by separate acquisition of the signals using the phases $\varphi_{1\mathrm{C}}$ and $\varphi_{1\mathrm{N}}$ shifted by 90 degrees. It should be noted here that the States method may be omitted by such TPPI operation that shifts both of the I and S resonances in the indirect dimension to one side (positive or negative) of the spectral region. Even though either the real or imaginary data sets alone suffice in this case, the required region of the spectrum and thereby the length of the data array is doubled, so that the experimental cost is unchanged.

In this way, the real and imaginary data sets $s^{(\xi)}_{\mathrm{real}}(t_1,t_2)$ and $s^{(\xi)}_{\mathrm{imag}}(t_1,t_2)$ are obtained for each of the ^{13}C and ^{15}N receiver channels ($\xi = (I = {}^{13}\mathrm{C}, S = {}^{15}\mathrm{N})$). By performing Fourier transformation with respect to t_2 followed by proper phase adjustment, we obtain arrays of 1D spectra

$$S^{(\xi)}_{\mathrm{real}}(t_1,\omega_{2\xi}) = \int s^{(\xi)}_{\mathrm{real}}(t_1,t_2)\exp(-i\omega_{2\xi}t_2)dt_2, \tag{1}$$

$$S^{(\xi)}_{\mathrm{imag}}(t_1,\omega_{2\xi}) = \int s^{(\xi)}_{\mathrm{imag}}(t_1,t_2)\exp(-i\omega_{2\xi}t_2)dt_2, \tag{2}$$

and thereby the hypercomplex data sets

$$S^{(\xi)}(t_1,\omega_{2\xi}) = \mathrm{Re}\{S^{(\xi)}_{\mathrm{real}}(t_1,\omega_{2\xi})\} + i\mathrm{Re}\{S^{(\xi)}_{\mathrm{imag}}(t_1,\omega_{2\xi})\}. \tag{3}$$

Up to this point, the procedures of 2D FT NMR and covariance NMR are identical. In the former, the second Fourier transformation is applied to Eq. (3), giving the conventional 2D spectra $S^{(\xi)}(\omega_1, \omega_{2\xi})$ represented by

$$S^{(\xi)}(\omega_1, \omega_{2\xi}) = \int S^{(\xi)}(t_1, \omega_{2\xi}) \exp(-i\omega_1 t_1) dt_1. \tag{4}$$

Note that, by appropriate TPPI implementation, the resonance frequencies of the I and S spin species in the indirect dimension are well separated, as schematically depicted in Fig. 2(a). Here, $S^{(I)}(\omega_{1I}, \omega_{2I})$ carries the correlations between the $I-I$ and $I-S$ spins, while $S^{(S)}(\omega_{1S}, \omega_{2S})$ exhibits the $S-I$ and $S-S$ correlations.

The covariance $C(X, Y)$ between two complex variables $X = \{x_1, \cdots, x_N\}$ and $Y = \{y_1, \cdots, y_N\}$ is defined as

$$\begin{aligned} C(X,Y) &= \frac{1}{N}\sum_{k=1}^{N}(X - \langle X\rangle)(Y - \langle Y\rangle)^* & (5)\\ &= \langle XY^*\rangle - \langle X\rangle\langle Y^*\rangle. & (6) \end{aligned}$$

Here, the asterisks and the brackets denote for complex conjugate and averaging. Now, we introduce covariances C^{II}, C^{IS}, C^{SI}, and C^{SS} calculated from the hypercomplex data sets $S^{(I)}(t_1, \omega_{2I})$ and $S^{(S)}(t_1, \omega_{2S})$ as

$$\begin{aligned} C^{II}(\omega_{2I}, \omega'_{2I}) &= \langle S^{(I)}(t_1, \omega_{2I}) S^{(I)}(t_1, \omega'_{2I})^*\rangle \\ &\quad -\langle S^{(I)}(t_1, \omega_{I2})\rangle\langle S^{(I)}(t_1, \omega'_{2I})^*\rangle, & (7)\\ C^{IS}(\omega_{2I}, \omega'_{2S}) &= \langle S^{(I)}(t_1, \omega_{2I}) S^{(S)}(t_1, \omega'_{2S})^*\rangle \\ &\quad -\langle S^{(I)}(t_1, \omega_{2I})\rangle\langle S^{(S)}(t_1, \omega'_{2S})^*\rangle, & (8)\\ C^{SI}(\omega_{2S}, \omega'_{2I}) &= \langle S^{(S)}(t_1, \omega_{2S}) S^{(I)}(t_1, \omega'_{2I})^*\rangle \\ &\quad -\langle S^{(S)}(t_1, \omega_{2S})\rangle\langle S^{(I)}(t_1, \omega'_{2I})^*\rangle, & (9)\\ C^{SS}(\omega_{2S}, \omega'_{2S}) &= \langle S^{(S)}(t_1, \omega_{2S}) S^{(S)}(t_1, \omega'_{2S})^*\rangle \\ &\quad -\langle S^{(S)}(t_1, \omega_{2S})\rangle\langle S^{(S)}(t_1, \omega'_{2S})^*\rangle, & (10) \end{aligned}$$

where the brakets indicate averaging over t_1. The covariance spectra $C^{\xi\xi'}$ $(\xi, \xi' = I, S)$ in Eqs. (7)-(10) correspond to the four regions of the 2D FT spectra, as depicted in Fig. 2(a)(b).

In practice, the acquired data sets are in the form of discrete data points. Accordingly, we rewrite $S^{(I)}(t_1, \omega_{2I})$ and $S^{(S)}(t_1, \omega_{2S})$ in Eq. (3) as

$$\begin{aligned} S^{(I)}(p\Delta t_1, q_I \Delta\omega_{2I}) &= S^{(I)}_{p,q_I}, & (11)\\ S^{(S)}(p\Delta t_1, q_S \Delta\omega_{2S}) &= S^{(S)}_{p,q_S}, & (12) \end{aligned}$$

where $p = 1, \cdots, N_1$, $q_I = 1, \cdots, N_I$, and $q_S = 1, \cdots, N_S$ are integers. Δt_1 is the increment of the evolution time. Note that Δt_1 and N_1 are common for I and S in the present work.

It is also possible to treat the data sets $S^{(I)}_{p,q_I}$ and $S^{(S)}_{p,q_S}$ as a single data set by joining them together into an array of 1D spectra $\mathbf{S}$, which is represented as

$$S_{p,q} = \begin{cases} S^I_{p,q}, & q = 1, \cdots, n_I \\ S^S_{p,q-n_I}, & q = n_I + 1, \cdots, n_I + n_S \end{cases}. \tag{13}$$

$\mathbf{S}$ is a $N_1 \times (n_I + n_S)$ matrix, from which the $(n_I + n_S) \times (n_I + n_S)$ covariance matrix $\mathbf{C}$ with elements

$$C_{ij} = \frac{1}{n_I + n_S - 1} \sum_{k=1}^{N_1} (S_{k,i} - \langle S_i \rangle)(S_{k,j} - \langle S_j \rangle)^* \tag{14}$$

are obtained with

$$\langle S_i \rangle = \frac{1}{n_I + n_S} \sum_{k=1}^{N_1} S_{k,i}. \tag{15}$$

As discussed in the previous works on covariance NMR, the covariance spectrum corresponds to the power spectrum in the 2D FT scheme. Thus, the square root $\mathbf{R}$ of the covariance matrix $\mathbf{C}$ gives a reasonable measure of the spin correlations. In general, calculation of $\mathbf{R}$ requires diagonalization of the covariance matrix. Due to the symmetric nature of $\mathbf{C}$, it is achieved by transformation using an orthogonal matrix $\mathbf{V}$ as

$$\mathbf{C} = \mathbf{V} \cdot \mathbf{D} \cdot \mathbf{V}^T, \tag{16}$$

where $\mathbf{D} = \mathrm{diag}(d_1, d_2, \cdots)$ is a diagonal matrix and $\mathbf{V}^T$ is the transposed matrix of $\mathbf{V}$. For orthogonal matrices, $\mathbf{V} \cdot \mathbf{V}^T = \mathbf{1}$. From the square root of $\mathbf{D}$, which is readily obtained as $\mathrm{diag}(\sqrt{d_1}, \sqrt{d_2}, \cdots)$, $\mathbf{R}$ is calculated by

$$\mathbf{R} = \mathbf{V}^T \cdot \sqrt{\mathbf{D}} \cdot \mathbf{V}. \tag{17}$$

Importantly, in the covariance approach, the resolution of $\mathbf{C}$ and thereby $\mathbf{R}$ along the indirect dimension is given by that of the direct dimension for any length $N_1 > 1$ of the t_1 increments. When the actual width of the peak of interest is less than the resolution given by the FT scheme, covariance becomes an attractive alternative to FT. Since much less N_1 suffices to extract spin correlations than that required in the conventional FT scheme, one can increase the number of signal accumulations within a given experimental time, leading to significant improvement in the attainable sensitivity.

EXPERIMENTAL

Solid-state NMR measurements were performed in a polycrystalline sample of uniformly ^{13}C, ^{15}N-labeled histidine. All experiments were carried out in a magnetic field of 9.4 T at room temperature using a Chemagnetics 3.2 mm MAS probe, which was triply tuned at the resonance frequencies of the ^{1}H, ^{13}C, and ^{15}N spins. For the dual receiver system, two OPENCORE NMR spectrometers[18–20] were used. One was devoted to ^{1}H and ^{13}C rf pulsing and ^{13}C detection, while the other was assigned to rf transmission and acquisition for the ^{15}N spins. They were triggered to be operated synchronously. The carrier frequencies were 400.2385 MHz, 100.650531 MHz, and 40.562604 MHz for the ^{1}H, ^{13}C, and ^{15}N resonances.

RESULTS AND DISCUSSION

Fig. 3 shows ^{15}N and ^{13}C CPMAS spectra of uniformly ^{13}C, ^{15}N-labeled histidine acquired simultaneously using the dual receiver system. The sample spinning frequency was 23 kHz, and, during the contact time of 200 μs, rf irradiation was applied with intensities of 60 kHz for the ^{1}H channel and 83 kHz for both the ^{13}C and ^{15}N channels. During the simultaneous signal acquisition, two pulse phase modulation (TPPM) decoupling[21, 22] was applied to the ^{1}H spins with an intensity of 100 kHz. In Fig. 3, the peaks are assigned according to ref. [23], and the IUPAC nomenclature is used for the labeling[24].

Typically, the ^{1}H-^{1}H dipolar coupling mediated ^{13}C/^{15}N chemical shift correlation experiments are performed with a contact time of the order of 100 μs, which is rather short compared to that used in the conventional CPMAS experiments. Appreciable peak intensities are thus expected for the protonated ^{13}C/^{15}N spins.

In order to optimize the correlation experiment for the histidine sample that we used in this work, we examined the contact time dependence of the ^{13}C/^{15}N peak intensities (Fig. 4). For the proton-bearing carbons, transient oscillations were observed[25] with periods ranging from ca. 120 to 150 μs (Fig. 4(a)). On the other hand, the buildups of the $^{15}N_{\pi}$ and $^{15}NH_3^+$ magnetizations were much slower, as shown in Fig. (b). Since the optimal contact times distributed, we set the best compromise for the contact times τ_{CP1} and τ_{CP3} in the ^{1}H-^{1}H dipolar coupling mediated ^{13}C/^{15}N chemical shift correlation experiment (Fig. 1) to be 200

μs.

Next, we examined ^{13}C/^{15}N to ^{1}H polarization transfer during the second CP time τ_{CP2} by observing depolarization of the ^{13}C/^{15}N magnetizations. As demonstrated in Fig. 4(c)(d), we found that 200 μs was also a reasonable value for the contact time τ_{CP2} for CP from the ^{13}C/^{15}N spins back to the ^{1}H spins.

Fig. 5(a) shows a 2D covariance spectrum of the ^{1}H-^{1}H dipolar coupling mediated ^{13}C/^{15}N chemical shift correlation experiment obtained in uniformly ^{13}C,^{15}N-labeled histidine using the pulse sequence depicted in Fig. 1. After acquiring the ^{13}C and ^{15}N FIDs, we performed Fourier transformation with respect to the direct dimension, and obtained the hypercomplex data sets according to Eqs. (11)-(12). Then, we joined them together to arrange the data matrix $\mathbf{S}$ (Eq. (13)), and finally, we calculated the covariance matrix $\mathbf{C}$ using Eq. (14).

In order to calculate the square root $\mathbf{R}$ of $\mathbf{C}$, we applied the Hausholder transformation on $\mathbf{C}$ into a tridiagonal matrix[26]. The matrix was then diagonalized by employing the Jacobi rotations. The square root $\mathbf{R}$ obtained in this way is shown in Fig. 5(b). The size of the matrix $\mathbf{C}$ was 1548×1548, and the calculation of its square root took 4.5 hours on a personal computer with a Core-i7 processor using a program that we have written for this purpose. The calculation of a matrix square root may be done much more efficiently using a singular value decomposition (SVD) scheme, as reported by Trbovic et al.[27].

The data were taken along the indirect dimension t_1 for 1.024 ms, which is much shorter than the T_2 values of ^{13}C/^{15}N spins. We thus expect that, in the conventional 2D FT, more data should be taken along t_1. In order to clarify this point, the same data sets were processed with 2D FT. As shown in Fig. 5(c), the 2D FT spectrum was accompanied by a number of ripples along the indirect dimension[28], in contrast to the covariance processing that resulted in the ripple-free spectra even with such truncated FIDs (Figs. 5(a)(b)). Fig. 5(d) shows another 2D FT spectra with 8 times longer acquisition along t_1 ($N_1 = 256$), but with a smaller number of accumulations by a factor of 8, so that the total experimental time was almost the same as those in Figs. 5(a)-(c). Figs. 6(a) and (b) show slices of the 2D FT spectra that are shown in Figs. 5(c) and (d). Indeed, the resolution has been improved significantly, however, at the cost of the lower sensitivity. Moreover, the disturbing ripples are still visible in the ^{15}N peaks.

Fig. 6(c) and (d) show slices of the covariance $\mathbf{C}$ and the square root $\mathbf{R}$ of the covariance spectra, showing that the relative intensities of the peaks in the 2D FT spectrum are closer

to those in **R**. As discussed by Brüschweiler[4], similarity of the square root **R** with the 2D FT spectrum, rather than that of the covariance spectrum **C**, is based on the Parseval's theorem, which states that

$$\int_{-\infty}^{\infty} dt f(t) g^*(t) \propto \int_{-\infty}^{\infty} d\omega F(\omega) G^*(\omega), \tag{18}$$

where $F(\omega)$ and $G(\omega)$ are the Fourier transformation of $f(t)$ and $g(t)$. In the present case, $S^{(\xi)}(t_1, \omega_{2\xi})$ in Eq. (3) corresponds to $f(t_1)$ and $g(t_1)$, and $S^{(\xi)}(\omega_1, \omega_{2\xi})$ in Eq. (4) corresponds to $F(\omega_1)$ and $G(\omega_1)$. That is,

$$\int dt_1 S^{(\xi)}(t_1, \omega_{2\xi}) S^{(\xi')}(t_1, \omega_{2\xi'})^* \propto \int d\omega_1 S^{(\xi)}(\omega_1, \omega_{2\xi}) S^{(\xi')}(\omega_1, \omega_{2\xi'}). \tag{19}$$

The right-hand side of Eq. (19) is equivalent to the element of the square of the 2D FT matrix. On the other hand, the left-hand side coincides with the covariance when $\langle S^{(\xi)}(t_1, \omega_{2\xi}) \rangle \sim 0$. This condition is met in most cases, as $S^{(\xi)}(t_1, \omega_{2\xi})$ oscillates with t_1 due to the TPPI implementation. It follows that the square root **R** of the covariance matrix gives a spectrum which corresponds to the 2D FT spectrum with an evolution time that is sufficiently longer than T_2.

In practice, we deal with discrete data sets, and the integral in Eq. (19) is replaced by a summation. In addition, the summation is taken over a finite length, in contrast to that the Parseval's theorem demands integration over an infinite range. We expect that, as increasing the length N_1 of the data set along the indirect dimension t_1, the covariance matrix **C** asymptotically gets closer to the square of the 2D FT spectrum with sufficient t_1 increments. In Fig. 7 plotted are the intensities of the cross peaks in the covariance spectrum for various data lengths N_1. We found that the cross peak intensities monotonically decreased, and converged as N_1 was increased. The criterion for how many N_1 points should take depends on the target of the study. When one intends to extract the same profile from the covariance spectrum as that of the 2D FT spectrum, one needs to verify convergence of the peak intensities with increasing N_1. Otherwise, much less N_1 would suffice, as demonstrated in Fig. 5. We also verified that the intensity of the cross peaks in the 2D covariance spectrum with $N_1 = 32$ increased with the mixing time τ_m, confirming the possibility of structural analysis using the covariance spectra even without their perfect agreement with the 2D FT spectra.

SUMMARY

In this work, we implemented ^{13}C-^{13}C, ^{15}N-^{15}N, and ^{13}C-^{15}N covariance solid-state NMR spectroscopy in a polycrystalline sample of uniformly ^{13}C, ^{15}N-labeled amino acid under MAS. To our knowledge, this is the first demonstration of the covariance NMR spectroscopy that includes heteronuclear correlations as well as homonuclear correlations. The calculation of heteronuclear covariance requires transverse magnetizations of both the I and S spin species during the detection period. In the present case of ^{1}H-^{1}H dipolar coupling mediated ^{13}C/^{15}N chemical shift correlation experiment, an NMR system equipped with the dual receiver channels can be exploited to acquire the ^{13}C and ^{15}N FIDs simultaneously. In this work, we operated two separate single-receiver NMR spectrometers synchronously.

Since the resolution of the covariance 2D spectrum in the indirect dimension is given by that of the detection dimension, much fewer amounts of data sets suffice to yield a satisfactory, ripple-free 2D spectrum compared to the case of the conventional 2D FT scheme. One can therefore save the experimental time, or enhance the sensitivity by increasing the number of signal accumulations within a given measurement time. It has also been shown that the square root of the covariance matrix is a reasonable measure of the cross-peak intensities, in accordance with the previous reports on homonuclear covariance NMR spectroscopy.

The concept of covariance has wide potential applications in the field of NMR spectroscopy. In covariance HOMCOR/HETCOR, an array of 1D spectra is firstly obtained, and then covariance is calculated between a data point at one frequency and that at another frequency. However, it would also be possible to take covariance between an array of measured data with non-experimental data. A recent example of such is the so-called phase covariance NMR[29, 30], which is not relevant for 2D correlation experiments but for simple 1D single pulse experiments. In phase covariance, a set of FIDs is acquired with various phases of the excitation pulse. By calculating the covariance between the data and the pulse phases, a spectrum that is similar to the conventional spectrum is obtained. When the incoherent signals, such as telecommunication radio waves, are contaminated in the NMR spectrum, the phase covariance approach effectively eliminates them.

Phase covariance NMR takes the covariance between arrays of measured data and experimental parameters (rf phase). It would also be possible to consider covariance between a

data array and a mathematical function. For example, covariance processing using a sinusoidal function would be similar to Fourier transformation. However, they are not equivalent, because the former and the latter are irreversible and reversible process. We plan to further study covariance data processing in NMR spectroscopy, so that we could look at a wide variety of NMR data from different angles.

---

* E-mail: takezo@kuchem.kyoto-u.ac.jp

[1] E. Kupce, R. Freeman, J. Magn. Reson. **162** (2003) 300–310.

[2] E. Kupce, T. Nishida, R. Freeman, Prog. Nucl. Magn. Reson. **42** (2003) 95–122.

[3] R. Brüschweiler, F. Zhang, J. Chem. Phys. **120** (2004) 5253–5260.

[4] R. Brüschweiler, J. Chem. Phys. **121** (2004) 409–414.

[5] I. Noda, Appl. Spectrosc. **47** (1993) 1329–1336.

[6] B. Hu, J.-P. Amoureux, J. Trebosc, M. Deschamps, G. Tricot, J. Chem. Phys. **128** (2008) 134502.

[7] M. Weingarth, P. Tekely, R. Brüschweiler, G. Bodenhausen, Chem. Comm. **46** (2010) 952–954.

[8] Y. Masuda, M. Fukuchi, T. Yatagawa, M. Tada, K. Takeda, K. Irie, K. Akagi, Y. Monobe, T. Imazawa, K. Takegoshi, Bioorg. Med. Chem. **19** (2011) 5967–5974.

[9] F. Zhang, R. Brüschweiler, J. Am. Chem. Soc. **126** (2004) 13180–13181.

[10] B. Hu, J.-P. Amoureux, J. Trebosc, Solid State Nucl. Magn. Reson. **31** (2007) 163–168.

[11] D.A. Snyder, Y. Xu, D. Yang, R. Brüschweiler, J. Am. Chem. Soc. **129** (2007) 14126–14127.

[12] D.A. Snyder, R. Brüschweiler, J. Phys. Chem. **A113** (2009) 12898–12903.

[13] O. Lafon, B. Hu, J.-P. Amoureux, P. Lesot, Chem. Eur. J. **17** (2011) 6716–6724.

[14] A. Lange, S. Luca, M. Baldus, J. Am. Chem. Soc. **124** (2002) 9704–9705.

[15] A. Lange, K. Seidel, L. Verdier, S. Luca, M. Baldus, J. Am. Chem. Soc. **125** (2003) 12640–12648.

[16] C. Herbst, K. Riedel, Y. Ihle, J. Leppert, O. Ohlenschläger, M. Görlach, R. Ramachandran, J. Biomol. NMR **41** (2008) 121–125.

[17] D.J. States, R.A. Haberkorn, D.J. Ruben, J. Magn. Reson. **48** (1982) 286–292.

[18] K. Takeda, Rev. Sci. Instrum. **78** (2007) 033103.

[19] K. Takeda, J. Magn. Reson. **192** (2008) 218–229.

[20] K. Takeda, Annual Reports on NMR Spectroscopy **74** (2011) 355–393.

[21] A.E. Bennett, C.M. Rienstra, M. Auger, K.V. Lakshmi, R.G. Griffin, J. Chem. Phys. **103** (1995) 6951–6958.

[22] Z. Gan, R.R. Ernst, Solid State Nucl. Magn. Reson. **8** (1997) 153–159.

[23] M.H. Frey, S.J. Opella, J. Magn. Reson. **66** (1986) 144–147.

[24] IUPAC-ICB Joint Commission on Biochemical Nomenclature. Pure Appl. Chem. **56** (1984) 595–624.

[25] B.-J. van Rossum, C.P. de Groot, V. Ladizhansky, S. Vega, M.J.M. de Groot, J. Am. Chem. Soc. **122** (2000) 3465–3472.

[26] W.H. Press, B.P. Flannery, S.A. Teukolsky, W.T. Vetterling, *Numerical Recipes in C: The Art of Scientific Computing, 2nd Edition*, Cambridge University Press (1993).

[27] N. Trbovic, S. Smirnov, F. Zhang, R. Brüschweiler, J. Magn. Reson. **171** (2004) 277–283.

[28] R.R. Ernst, G. Bodenhausen, A. Wokaun, *Principles of Nuclear Magnetic Resonance in One and Two Dimensions*, Oxford (1987).

[29] J. Fukazawa, K. Takegoshi, Phys. Chem. Chem. Phys. **12** (2010) 11225–11227.

[30] J. Fukazawa, K. Takeda, K. Takegoshi, J. Magn. Reson. **211** (2011) 52–59.

Figure Captions

Figure 1

A pulse sequence for ^{1}H-^{1}H dipolar-coupling mediated ^{13}C/^{15}N chemical shift correlation experiments. The signals from the ^{13}C and ^{15}N spins are acquired simultaneously. Time proportional phase increment (TPPI) is applied to phases $\varphi_{1\mathrm{C}}$ and $\varphi_{1\mathrm{N}}$. That is, $\varphi_{1\mathrm{C}} = \varphi_{0\mathrm{C}} + t_1\Delta\varphi_{1\mathrm{C}}$ and $\varphi_{1\mathrm{N}} = \varphi_{0\mathrm{N}} + t_1\Delta\varphi_{1\mathrm{N}}$, and the freqency shift in the indirect dimension is determined by $2\pi/\Delta\varphi_{1\mathrm{C}}$ and $2\pi/\Delta\varphi_{1\mathrm{N}}$, respectively. In addition, a quadrature pair of data are acquired for a given value of t_1, with $\varphi_{0\mathrm{C}}$ and $\varphi_{0\mathrm{N}}$ shifted by $\pi/2$. For the real part of the hypercomplex data, the phases are cycled as follows. $\varphi_{0\mathrm{C}}, \varphi_{0\mathrm{N}} : x, x, -x, -x$; $\varphi_2 : x, -x, x, -x$; $\varphi_3 : -y, -y, y, y$; $\varphi_{\mathrm{acq}} : -y, y, -y, y$. For the imaginary part of the hypercomplex data, the phases are cycles as follows. $\varphi_{0\mathrm{C}}, \varphi_{0\mathrm{N}} : -y, -y, y, y$; $\varphi_2 : x, -x, x, -x$; $\varphi_3 : x, x, -x, -x$; $\varphi_{\mathrm{acq}} : x, -x, x, -x$.

Figure 2

Correspondence between (a) the 2D FT spectra $S^{(I)}(\omega_{1I}, \omega_{2I})$, $S^{(S)}(\omega_{1S}, \omega_{2S})$ and (b) the covariance spectra $C^{II}(\omega_{2I}, \omega'_{2I})$, $C^{IS}(\omega_{2I}, \omega'_{2S})$, $C^{SI}(\omega_{2S}, \omega'_{2I})$, and $C^{SS}(\omega_{2S}, \omega'_{2S})$.

Figure 3

(a)(b) ^{15}N and ^{13}C CPMAS spectra of uniformly ^{13}C-^{15}N labeled histidine acquired simultaneously using the dual receiver system. The contact time was 200 μs, and the signals were accumulated over 40 times under MAS at 23 kHz. (c) The structure of histidine. The carbon and the nitrogen sites are labeled according to IUPAC nomenclature.

Figure 4

Measured polarization and depolarization curves of (a)(c) ^{13}C peaks and (b)(d) ^{15}N peaks. In (a) and (b), the buildup behavior of the ^{13}C and ^{15}N magnetizations are plotted as a function of the contact time τ_{CP1}. In (c) and (d), the ^{13}C and ^{15}N magnetizations were firstly enhanced by CP with a contact time of 200 μs. After eliminating the ^{1}H magnetization by a z-filter, the second CP was applied with various contact times τ_{CP2}, aiming at transferring the ^{13}C and ^{15}N magnetizations back to the ^{1}H spins. The experiments were carried out in a magnetic field of 9.4 T under MAS at 23 kHz.

Figure 5

(a) A 2D covariance spectrum of ^{1}H-^{1}H dipolar coupling mediated ^{13}C/^{15}N chemical shift correlation experiment obtained in uniformly ^{13}C, ^{15}N-labeled histidine with the pulse sequence described in Fig. 1. The experimental parameters are as follows. $\tau_{\mathrm{CP1}} = \tau_{\mathrm{CP2}} = \tau_{\mathrm{CP3}} = 200$

μs, τ_d = 3 ms, τ_m = 200 μs. t_1 was incremented by 33 μs up to 1.024 ms, so that the length N_1 of the data sets was 32. TPPI was applied to shift the frequencies in the indirect dimension by -5 kHz and +10 kHz for the ^{13}C and ^{15}N channels, respectively. The signals were accumulated over 320 times with a recycle delay of 3 s. The experiment was carried out in a magnetic field of 9.4 T under MAS at 23 kHz. The data was processed according to the procedure described in the text, and plotted with 5 contours whose heights range from 2.0% to 50% of the highest peak. (b) The square root **R** of the 2D covariance spectrum in (a). (c) A 2D FT spectrum using the identical data sets used in (a)(b). (d) A 2D FT spectrum obtained with 256 t_1 increments up to 8.416 ms, which was 8 times that of the data in (c), whereas the number of accumulation was reduced by a factor of 8 (i.e., 320/8=40), to make the total measurement time the same.

Figure 6

Slice spectra of (a) the 2D FT spectrum with N_1 = 32, (b) the 2D FT spectrum with $N_1 = 64$, (c) the covariance spectrum, and (d) the square root of the covariance spectrum. The same data sets were used as those plotted in Fig. 5. The slices were taken along the indirect dimension t_1 at the peaks corresponding to the C_β, C_α, C_5, C_2, NH_3^+, and N_τ atomic sites.

Figure 7

Array-length dependence of the intensities of the cross peaks in the 2D covariance spectra of ^{1}H-^{1}H dipolar coupling mediated ^{13}C/^{15}N chemical shift correlation experiment. The experiment was carried out with an array length of 256, and the covariance processing was performed for various lengths N_1 of the data sets taken from the acquired data. The MAS frequency was 23 kHz, and the mixing time τ_m was 200 μs. (a), (b), and (c) show the cross-peak intensities for the ^{13}C-^{13}C, ^{13}C-^{15}N, and ^{15}N-^{15}N correlations, respectively.

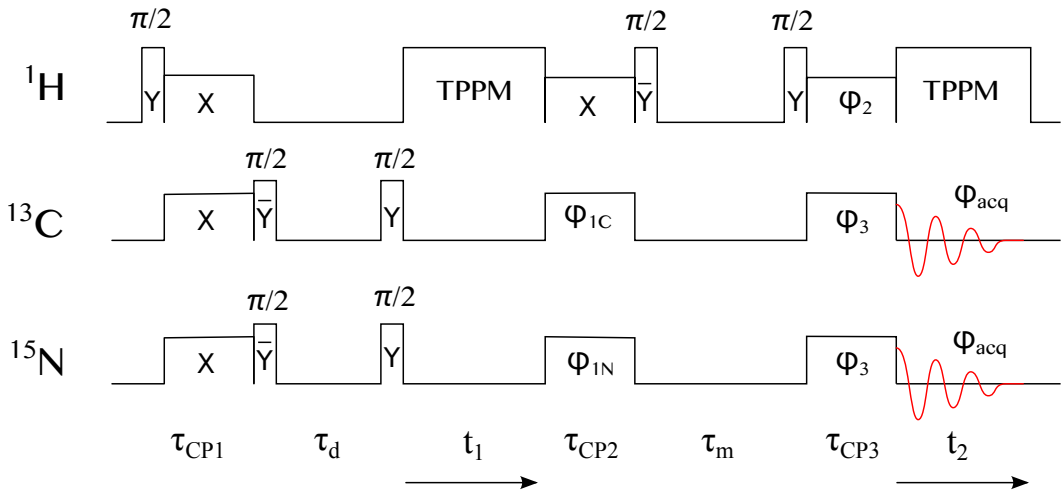

Fig. 1

Takeda et al.

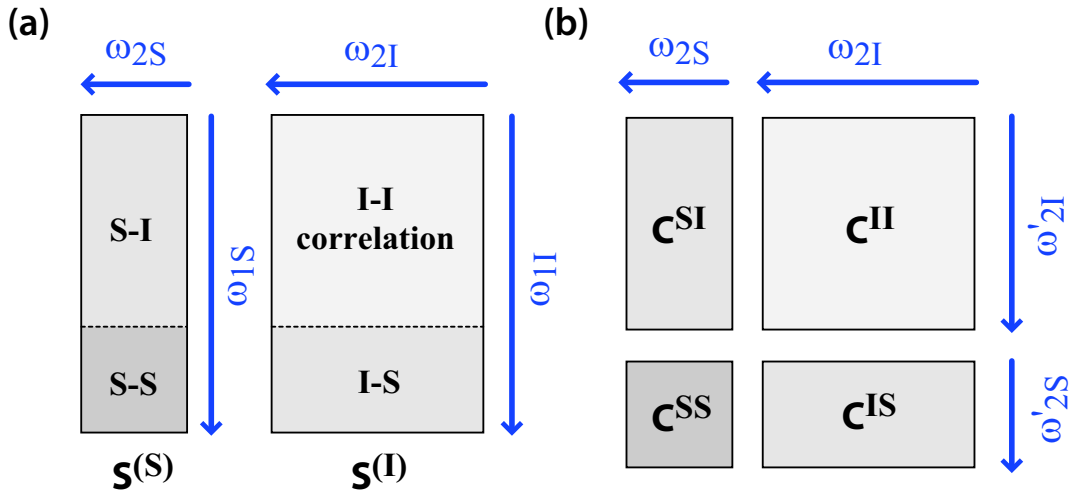

Fig. 2

Takeda et al.

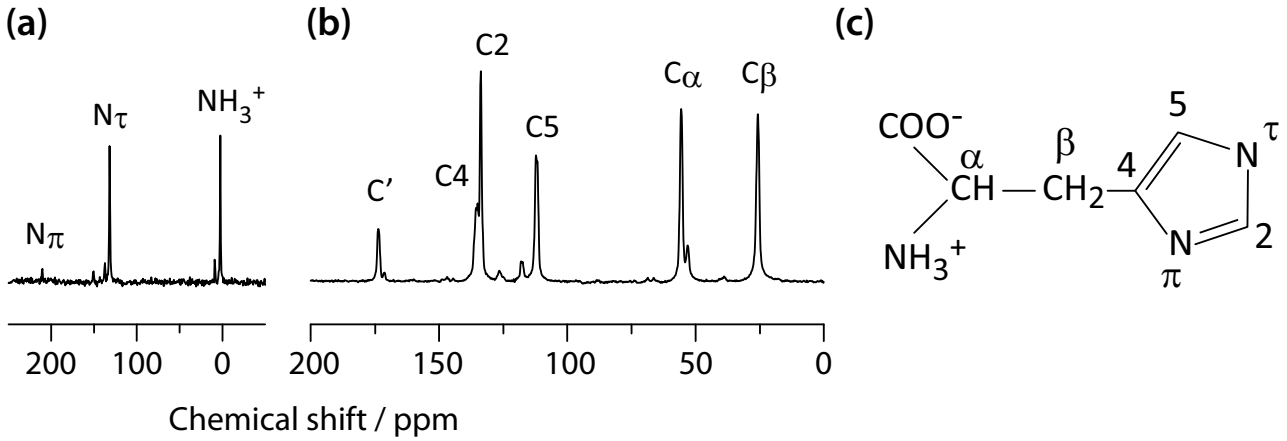

Fig. 3

Takeda et al.

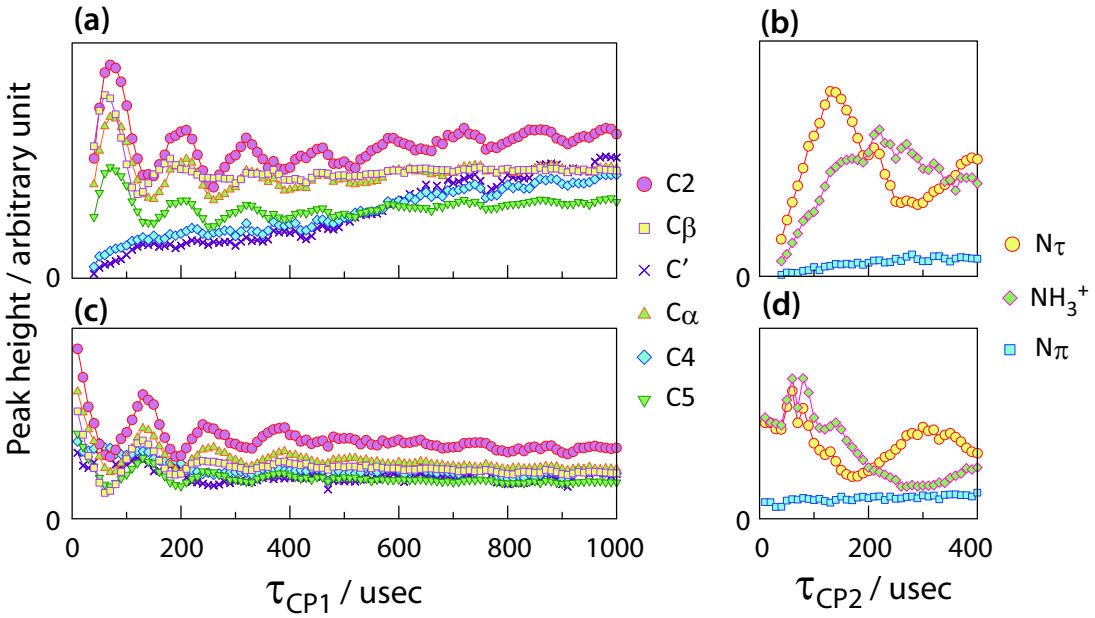

Fig. 4

Takeda et al.

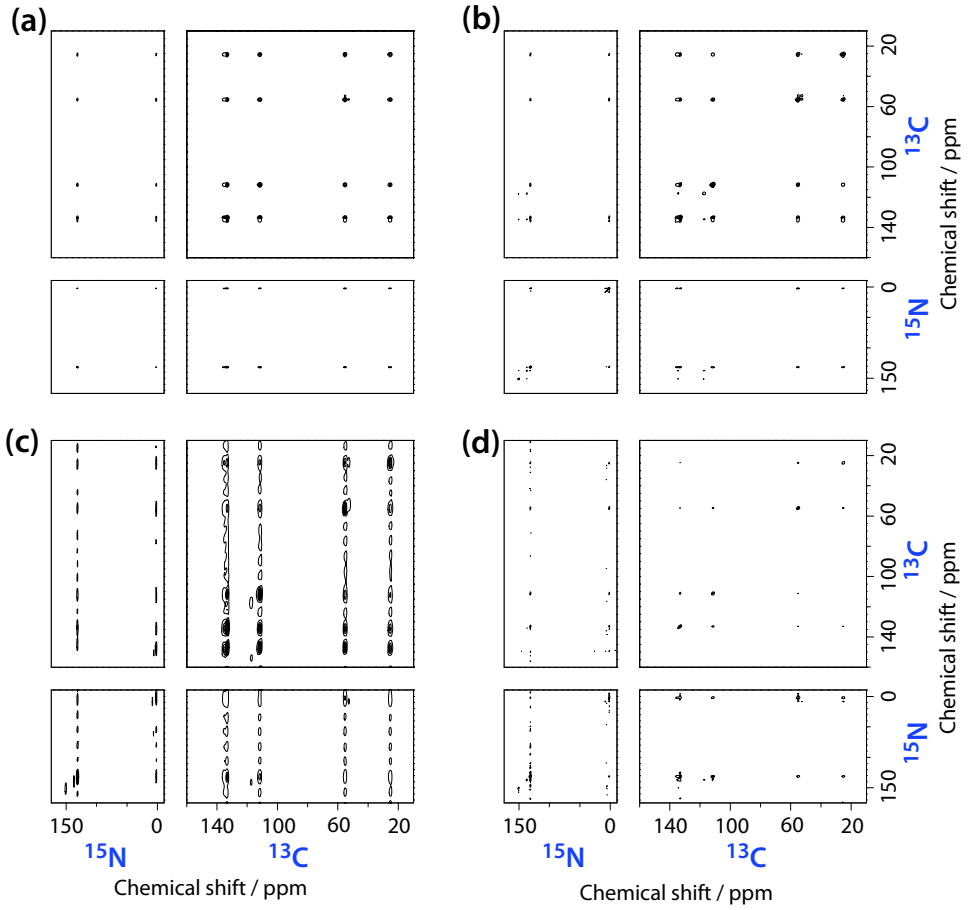

Fig. 5

Takeda et al.

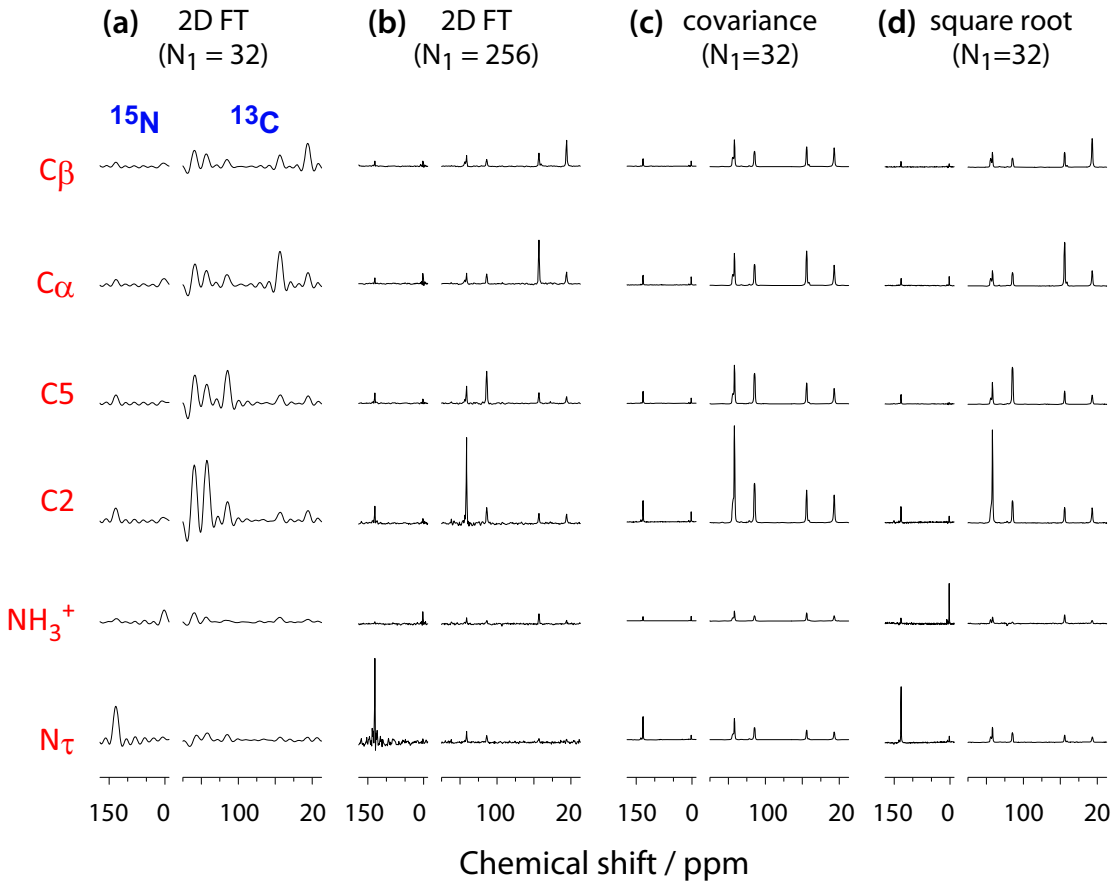

Fig. 6

Takeda et al.

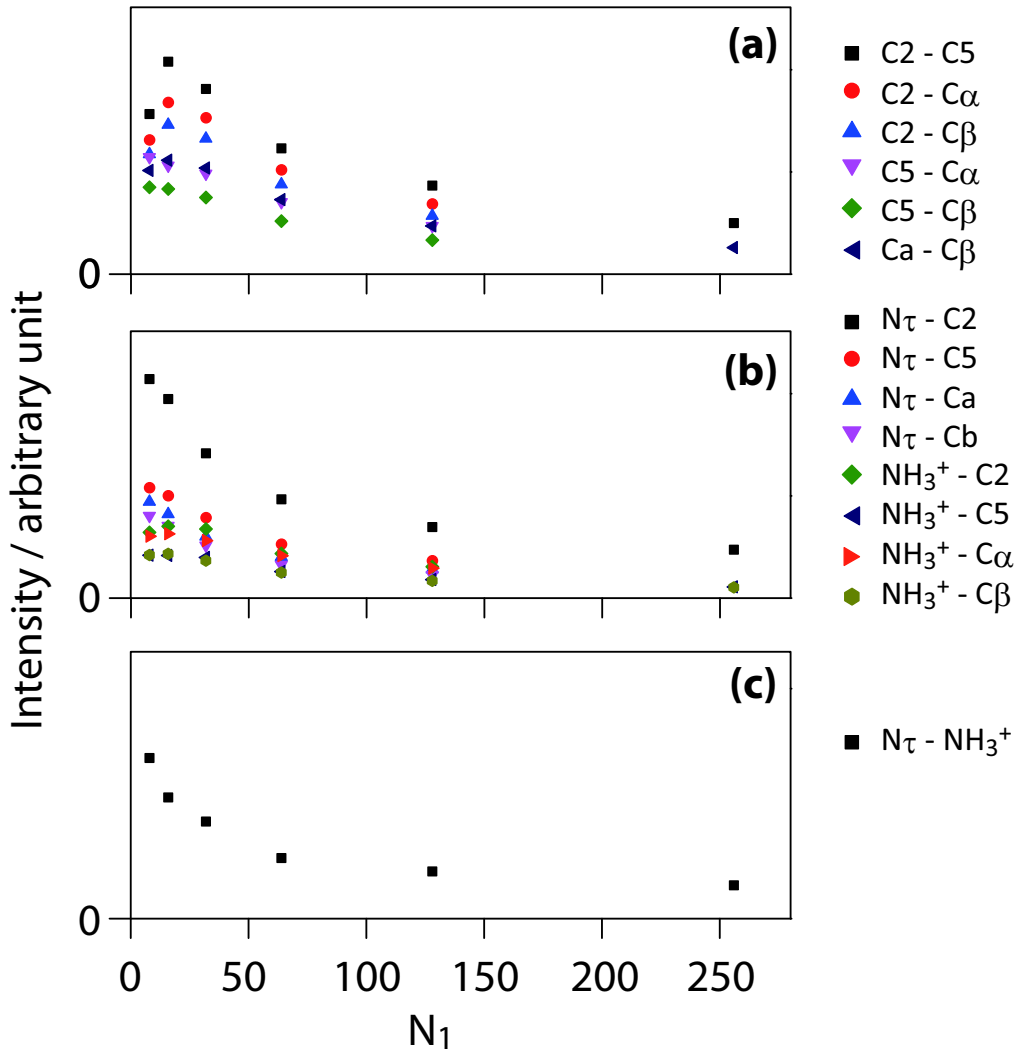

Fig. 7

Takeda et al.